Supporting Information

Enhanced performance of phase change memory by grain size reduction

Yuan Xue*, Sannian Song*, Xiaogang Chen, Shuai Yan, Shilong Lv, Tianjiao Xin, Zhitang Song*

Figure S1. BF TEM images and the raw integrated diffraction curves of electronic diffraction intensity extracted from the respective SAED patterns for (a)-(b) GST and (c)-(d) TaGST films.

Figure S2. In-situ XRD results for GST and TaGST films.
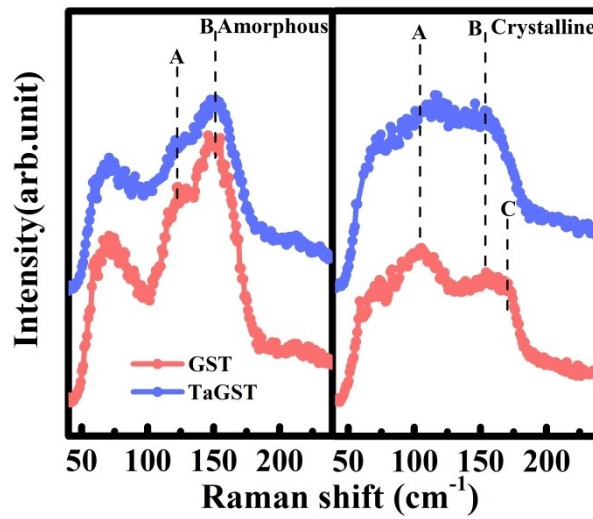
Figure S3. Raman spectra for amorphous and crystalline GST and TaGST films.
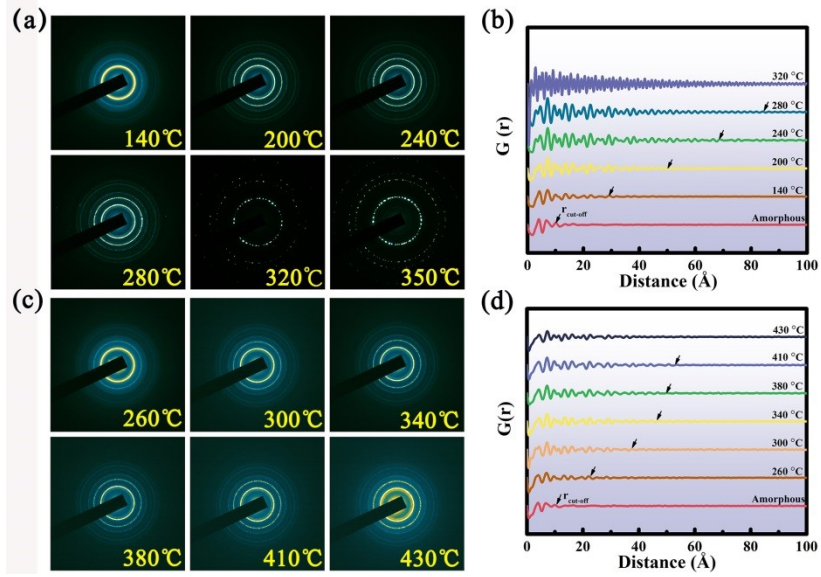
Figure S4. Evolution of selected area electron diffraction patterns and the corresponding real-time radial distribution function G(r) curves of (a)-(b) GST and (c)-(d) TaGST at *r* ranging from 2 to 100 Å.
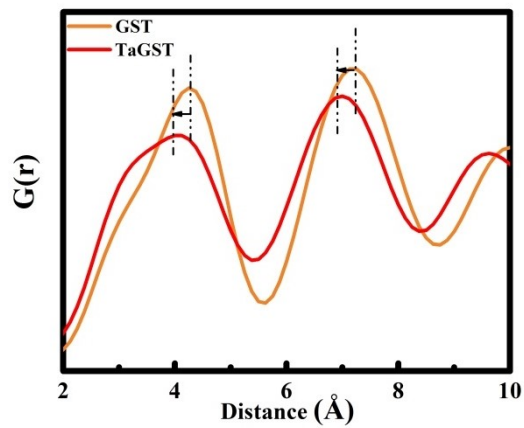
Figure S5. Evolution of real-time radial distribution function G(r) curves at *r* ranging from 2 to 10 Å for as-deposited films.

3
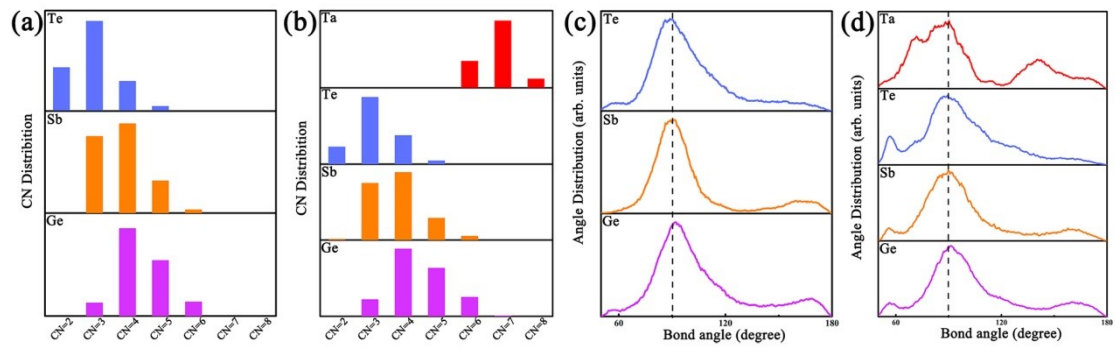
Figure S6. (a)-(b) Coordination number distribution and (c)-(d) the bond angle distribution of Ge, Sb, Te and Ta for amorphous GST and TaGST.
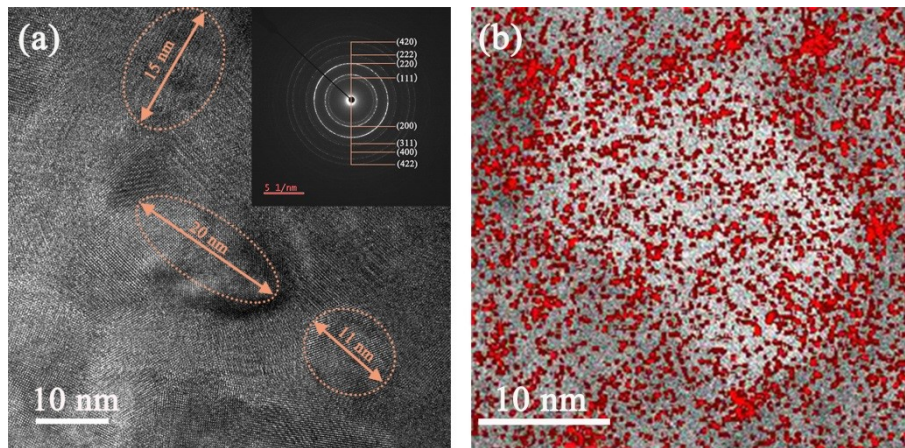
Figure S7. (a) HRTEM image of TaGST film after 400 °C for 20 min. (b) Ta element is distributed in a complete grain of TaGST film after annealed at 400 °C for 20 min.
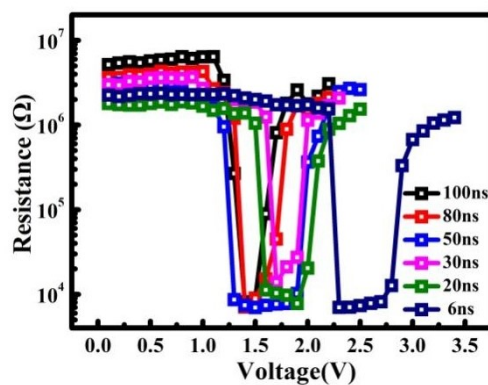
Figure S8. The R-V of the device based on TaGST.
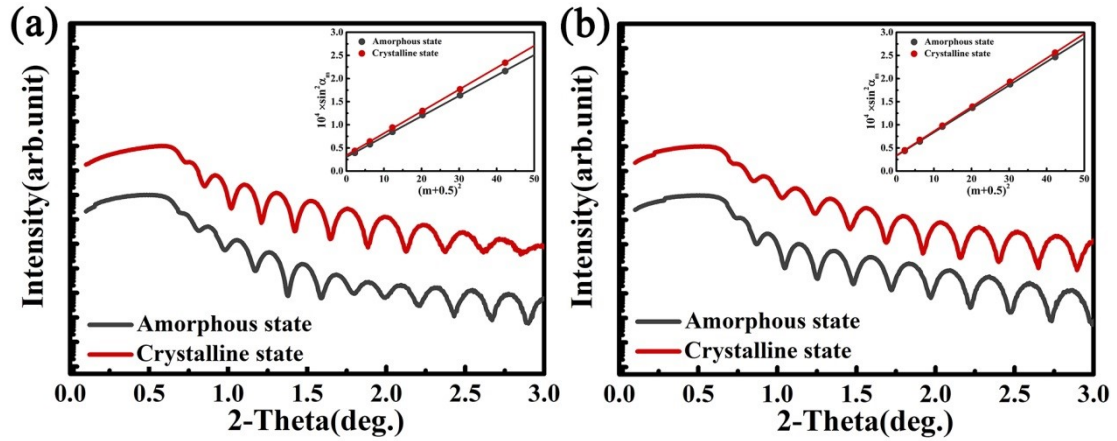
Figure S9. XRR patterns for a) GST, b) TaGST films. The insets are the plot of $\sin^2\theta$ versus $(m + 0.5)^2$ films.
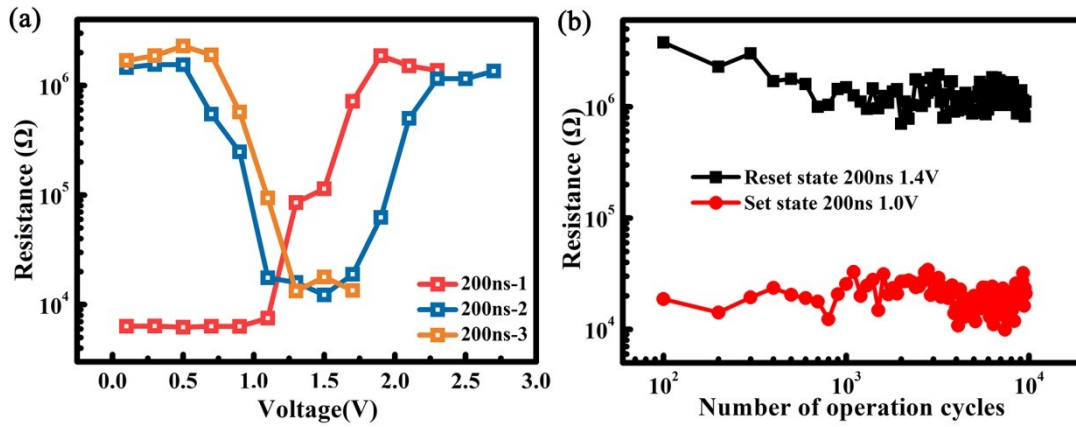
Figure S10. (a) The R-V of the sample 1. (b) Endurance of the sample 2.
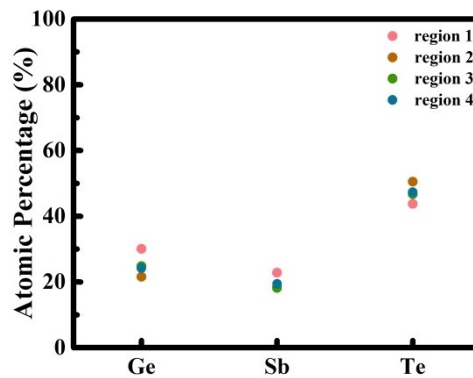
Figure S11. The variation tendency of basic element contents for regions 1-4 of the sample 2.